Synthesis and characterization of manganese-doped FeS_2 thin films via chemical spray pyrolysis

R. S. Ali[a,*], H. S. Rasheed[b], N. F. Habubi[c], S. S. Chiad[b]
[a]*Department of Physics, College of Science, Mustansiriyah University, Baghdad, Iraq*
[b]*Department of Physics, College of Education, Mustansiriyah University, Baghdad, Iraq*
[c]*Department of Engineering of Refrigeration and Air Conditioning Technologies, Alnukhba, University College, Baghdad, Iraq*

A thin film of iron disulfide (FeS_2) and Mn-doped was prepared using the chemical spray pyrolysis (CSP) method at a constant temperature of the glass substrate at around 400 °C. According to XRD examination, films were structurally cubic oriented with a predominant planar orientation (201). The doping of Mn ions in the FeS_2 host matrix was confirmed by a minor shift of the diffraction peak towards the lower 2θ values. The surface of the produced film for pyrite was homogeneous, according to the AFM investigations. According to the XRD data, the predicted grain size altered as the consistent manganese increased. When compared to undoped FeS_2 thin films, the Mn^{2+}-doped FeS_2 thin films' desired bandgap energy showed a red shift.

(Received October 19, 2022; Accepted January 17, 2023)

Keywords: FeS_2, Mn: thin films, Chemical spray pyrolysis, Structure, Topography, Optical properties, E_g.

1. Introduction

Due to its favorable bandgap (0.95 eV) and high absorption coefficient (> 10^5 cm^{-1} for wavelengths about 10^3 nm), FeS_2 iron pyrite is widely applied [1–2]. Two more structures exist in FeS_2: cubic pyrite (-FeS2) and rhombic marcasite (-FeS_2).Two types of FeS can be produced, FeS_2 can be an n-type and/or p-type semiconductor depending on the growth conditions and the type of impurities. At low temperatures, it can form P-type FeS_2 and S/Fe ratio > 2, but FeS_2 with n-type conductivity can be formed under high temperatures and iron-rich conditions [3, 4].

Researchers have conducted several extensive experiments on the impact of doping on the pyrite films' characteristics [5]. Extensive focus has been placed on studying the impact of doping on electronic properties. Research has proven that some researchers obtained pyrite thin films doped with other elements, such as nickel and copper, synthesized experimentally [6, 7]. The energy gap values can be changed to suit the application. Successful doping of different elements in FeS_2 has been reported to improve properties by saturating materials [8-11]. Therefore, to modify the energy gap of FeS_2, some materials, such as Mn are chosen as the doping agent. Several methods were used to produce thin films, such as the hydrothermal method [12], melt thermal method [13], microwave production method [14], and co-deposition method with polymer [15] for the synthesis of nanophase pyrite from FeS_2 with various shapes. Additionally, FeS2 thin-film was prepared using a variety of techniques, including electrodeposition [16], thermal deposition [17], CSP [18], spin coating [19], magnetron spraying [20], microwave-assisted method [21] and CVD [22], In the current study, FeS_2 is doped with manganese was synthesis by simple chemical spray pyrolysis (CSP) .The impact of impurity on many properties of films such as stoichiometric, structure, morphology, and optical properties are studied.

* Corresponding author: reemphy81@uomustansiriyah.edu.iq
https://doi.org/10.15251/CL.2023.201.63

2. Experimental

$FeCl_2$ and thiourea CS $(NH_2)_2$ are employed in a straightforward method to generate thin films of FeS_2 iron pyrite by CSP. The prepared solution has a molarity of 0.1 M. Thiourea is dissolved in deionized water, $FeCl_2$ was resolved in a 1:1 mixture of methanol and re-distilled water. A few drops of HCl were added to make $FeCl_2$ better solubility. The activating agent was Mn trichloride ($MnCl_3$) diluted in deionized water. The prepared solutions of iron chloride and thiourea were well combined to obtain a Fe:S ratio of 1:2. Filtered air preserved at a pressure of 10^5 N/m, flowing at a rate of 5 mL/min, was used to spray the previously prepared solutions onto glass substrates. A waiting interval of 2 minutes was included after the spraying process to prevent overcooling.The base temperature was constant at 400°C, while the distance between the spout to the base was fixed at about 29 cm. Under these deposit conditions, good films are obtained. It is homogeneous and very adherent to the substrates. The transmittance was measured with a dual-beam spectrophotometer. XRD obtained structural properties. AFM (was used to examine the films' surface.

3. Results and discussions

Regarding the exceptional structural results, Figure 1 offers the XRD styles of the deposited films at 2θ ranging from 10 to 70°, where all peaks are well shown to be FeS_2 cubic pyrite (JCPDS Card No. 710053). The XRD patterns reveals a modest shift (0.02°) of the major characteristic peaks (201) carried on by Mn incorporation into the FeS_2 structure in the doping samples. According to the given calculations, the lattice parameter would rise when Mn^{2+} (0.08 nm), which has an ionic radius higher than Fe^{2+} (0.074 nm), was integrated into the FeS_2 structure, generating an alternate solid solution [23,24]. Additionally, the 2% and 4% doping samples' (201) diffraction peak intensities are greater than the pure sample, suggesting that the films grew with (201) a favored orientation.

The films have five distinct diffraction peaks, at 2θ of 32.92°, 36.92, 47.28°, 56.12° and 61.19° attributed to the (200), (201), (220), (221) and (321) planes respectively. Using Scherer's equation [25,26], the average crystallite size (D) was computed via relation below:

$$D = \frac{0.9\lambda}{\beta cos\theta} \tag{1}$$

where β is the FWHM and λ is the X-ray wavelength. D were found to be 10.21–11.31 nm and is shown in Table 1.

The microstrain (ε) and dislocation density (δ) were calculated by using the following (Eqs. 2 and 3) [27, 28], and their values are given in Table 1.

Microstrain

$$(\varepsilon) = \frac{\beta cos\theta}{4} \tag{2}$$

dislocation density

$$(\delta) = \frac{1}{D^2} \tag{}$$

Doping leads to network stress in FeS_2 thin films. We notice an increase in the lattice parameter values of the cubic doped membranes monotonously with the doping, which led to microscopic stress in the cubic structure of pyrite. All of the doped films were found to have higher values than the FeS_2 values ($3.39\ 10^{-3}$) that arise from cation substitution, which agrees with the 3.4×10^{-3} values for pyrite thin films previously reported that were estimated by [29, 30]. Two metal ions in the pyrite lattice have different diameters, which results in the deformation of the lattice. Particularly, the dislocation's density and the precise stress brought on by the transition metal's doping are inversely related. Alternative solid solutions are the films made from non-

ductile pyrite thin films placed on glass substrates that contain divalent cations with ionic radii higher than Fe^{2+} in the FeS_2 structure.

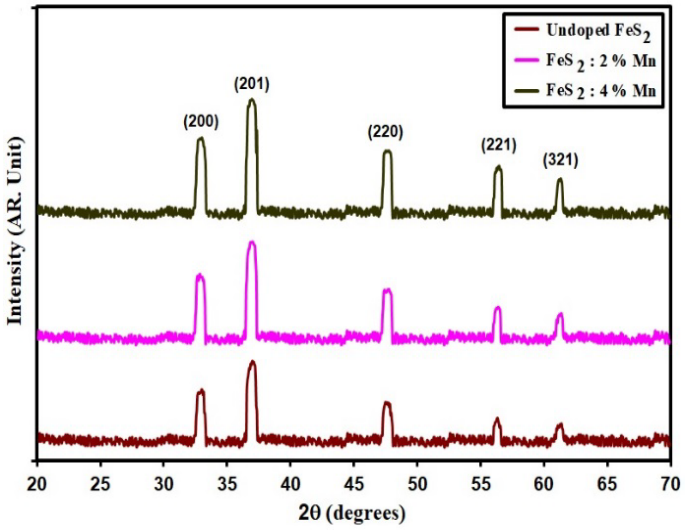

Fig. 1. XRD patterns of pure and FeS_2:Mn films with various doping.

Table 1. Structure parameter of pure and FeS_2:Mn films with various doping.

Specimen	2 □ (°)	(hkl) Plane	FWHM (°)	E_g (eV)	D (nm)	δ (× 10^{15}) (lines/m^2)	ε x10^{-3}
Undoped FeS_2	36.92	210	0.82	2.00	10.21	9.59	3.39
FeS_2: 2% Mn	36.89	210	0.78	1.94	10.74	8.66	3.22
FeS_2: 4% Mn	36.86	210	0.74	1.88	11.31	7.81	3.06

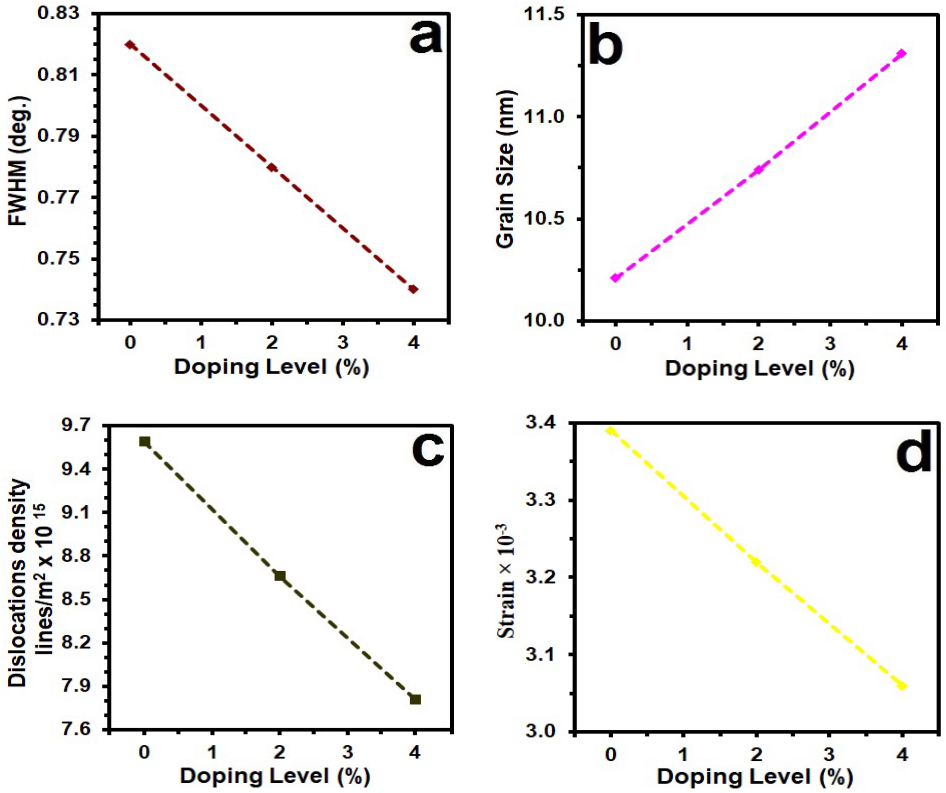

Fig. 2. X-ray parameters of the entended films.

4. Topography surface analysis

The existence of homogeneous, crack-free surfaces is confirmed by surface analysis of he thin films of (FeS_2) thin films that are saturated with transition metals. Surface roughness is related to the morphology, texture, and fine crystal quality. With a concentration of the doped and transition metal precursors, the surface roughness of transitional metal pyrite (Mn) (FeS_2) thin films deviates. The smoothness of the surfaces appeared on the thin films of pyrite saturated with manganese.

Figure 3 shows the effect of impurity concentration on the surface texture varies from granular growth to spherical growth of particles. On top of that, AFM parameters such as roughness modulus and average particle size were calculated. We observe the low values of nm RMS roughness at 3% doping which can be assinged to the decrease in crystal size with increasing doping content. Surface morphology plays a vital role in PV devices [31, 32]. The transition metal-doped (FeS_2) thin films' AFM height profiles indicate a uniform distribution of nanoparticles with an average particle height of 42.86 nm (Fig. 3). For transition metal-doped pyrite films, AFM results for scanning areas spanning from 78 nm 78 nm 21 nm scale indicated smooth surfaces with root mean squared (RMS) roughness values of 7.63 nm and 4.35 nm for 2and 4% doping in Mn (Figure 4). These Mn-doped smooth films exhibit microstrain values that are comparable to those of FeS_2, indicating that microstrain and overall film smoothness may be related [33] Table 2. AFM parameter measurement of pure and FeS_2: Mn films with various doping.

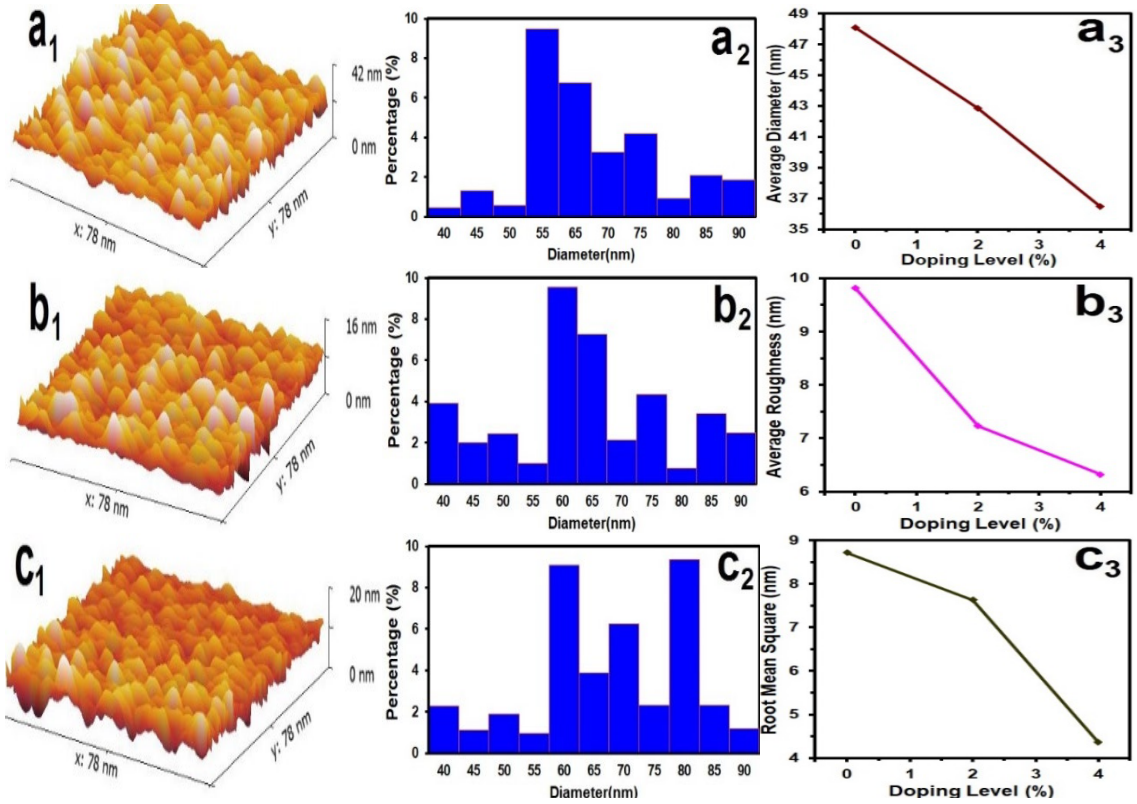

Fig. 3. AFM of pure and and FeS_2: Mn films with various doping.

Table 2. AFM parameters of the intended films.

Samples	Average Particle size nm	R_a (nm)	R. M. S. (nm)
Undoped FeS_2	48.08	9.81	8.72
FeS_2: 2% Mn	42.86	7.23	7.63
FeS_2: 4% Mn	36.46	6.34	4.35

5. Optical properties analysis

Fig. 4 shows the transmittance T as a function of λ. All samples displayed better transparency in the (600-900 nm) range than in the visible and NIR regions but a lower transmittance throughout the entire spectrum than the undoped films. This behavior suggests that doped pyrite films have a higher capacity for light absorption than doped pyrite films. Absorption coefficient (α) of the pure and FeS_2: Mn films were studied, and Lambert's law could be used to calculate α [34,35]:

$$\ln \frac{I_o}{I} = 2.303 = \alpha d \tag{4}$$

where Io and I, respectively, stand for the incident and transmitted light intensities. The optical absorbance is A, and the film thickness is d.

(α) versus photon energy (hν) curves shown in Fig. 5 the absorption coefficients of the samples in the range values of 2.75 $\times 10^3$ cm^{-1} and 3.75 $\times 10^5$ cm^{-1}, respectively, exhibits a significant divergence in the optical absorption characteristics. For Mn doped FeS2 thin films, a minor red shift in the bandgap was seen. Generally speaking, an increase in crystallite size can be linked to a decrease in optical band gap [36].

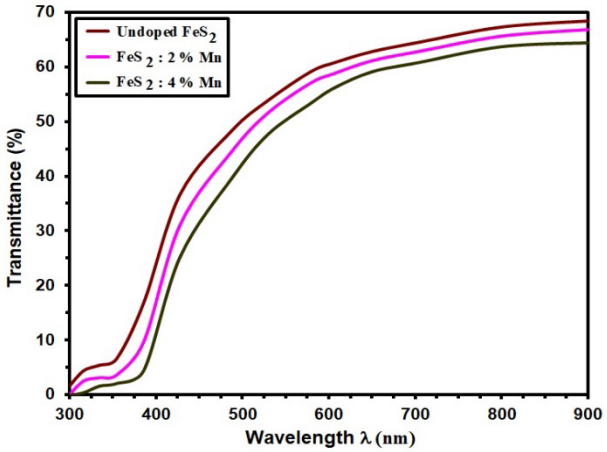

Fig. 4. Transmittance spectra of the entended films.

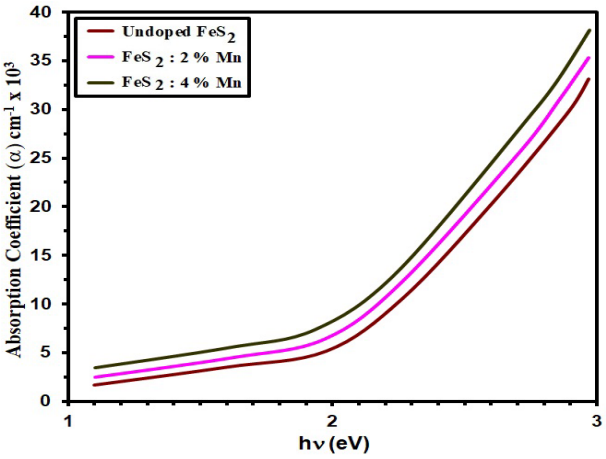

Fig. 5. α spectra of the entended films.

The bandgap energy Eg of these films has been determined based on the absorption spectra utilizing the relation [37,38]:

$$\alpha h\nu = k(h\nu - E_g)^{\frac{1}{2}} \tag{5}$$

where k a constant. The Eg values of the produced films with varying Mn-doped ratios are depicted in Fig. 6. For 2% and 4% doping in Mn, respectively, the band gap Eg of undoped sample was 2.00 eV and 1.94 1.88 eV. The Eg values have lowered as the doping concentration has increased. The sp-d interaction may be to responsible for this [39,40]. The band electrons and localized d electrons of Mn^{2+} substituting Fe^{2+} interact via a sp-d exchange process, decreasing the band gap. Mn^{2+} inclusion could redshift, leading to higher local states and a lower bandgap energy. We observe a redshift of the band edge as the uptake of Mn content within the membranes increases. The explanation behind this phenomena cause widening the Burstein-Moss bandgap and narrowing the bandgap due to the scattering of electron and electron impurities. In this study, the crystal size and crystallization increase was responsible for decreasing the band gap.

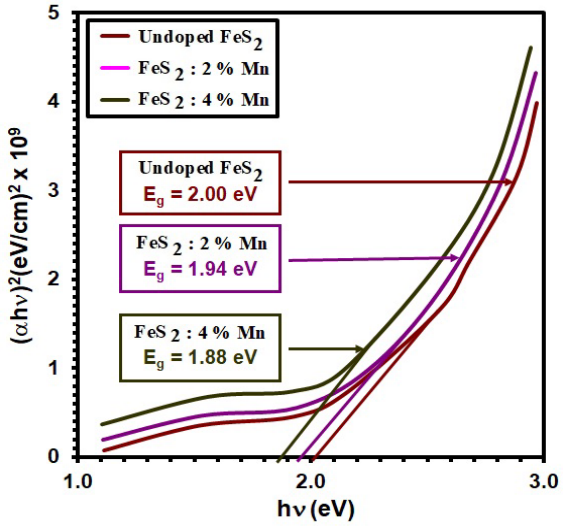

Fig. 6. Band gap of the entended films.

Using the connection (6 and 7) [41], the refractive index (n) and the extinction coefficient may be calculated from the reflectance (R) data:

$$R = \frac{(n-1)^2}{(n+1)^2} \tag{6}$$

$$K = \frac{\alpha\lambda}{4\pi} \tag{7}$$

Figures (7 and 8) represent n and k of the thin film samples. n shows a well dispersive nature for each sample, and the value increases to its highest point at a particular energy, leading that energy has been strongly polarized. After reaching its maximum, the value of n declines when photon energy characteristics increase due to multiple loss mechanisms being involved. It should be mentioned that the electrical density and local polarizability of the examined thin films are correlated. The value of n at 550 nm is obtained to be ~3.40, FeS_2 3.35 and 3.29 for pure and Mn-doped FeS_2 thin films, respectively. The value of n decreases with increasing Mn doping related to the well-known inverse width of the optical band gap. The observed drop in n and k with wavelength increase may be associated with the rise in transmittance and fall in absorption coefficient. Optic parameter variations have been observed to be similar [42,43].

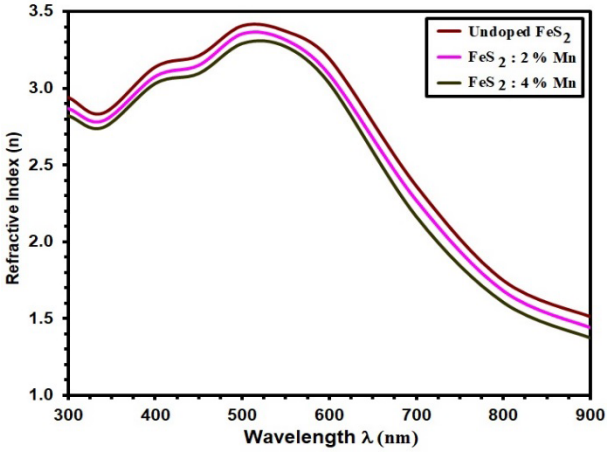

Fig. 7. n of the entended films.

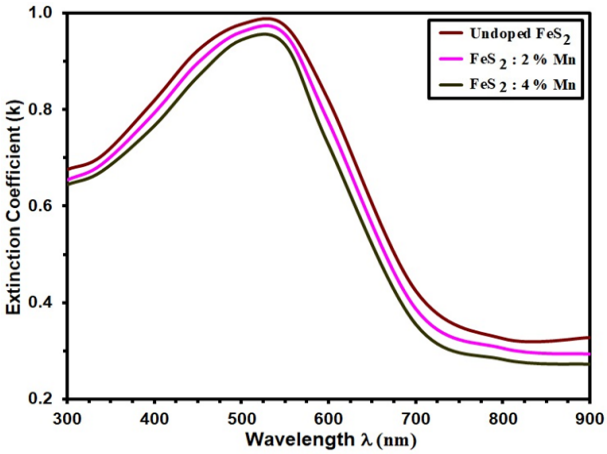

Fig. 8. K of the entended films.

6. Conclusion

FeS_2 films were successfully prepared by (CSP) at 400°C with various Mn concentrations. Mn-doped FeS_2 films revealed a minor shift in 2θ and a preferred orientation of (201) for all films. The doped Mn concentrations had a minor impact on the grain size of the resulting doped films. Transition pyrite (FeS_2) thin films' AFM height profiles reveal a homogeneous distribution of nanocrystalline particles with average particle heights of 48.08 nm and 42.86 nm when doped with 4% Mn metal. For (0, 2 and 4% doping in Mn, respectively, optical tests showed a drop in the bandgap of FeS_2 thin films from 2.00 eV and 1.94 1.88 eV.

Acknowledgements

Mustansiriyah University (www. uomustansiriyah.edu.iq) and Alnukhba University College support this work.

References

[1] A.Ennaoui, S. Fiechter, H. Goslowsky et al. J. Electrochem. Soc., 132: 1579(1985); https://doi.org/10.1149/1.2114168

[2] I.J.Ferrer, D.M. Nevskaia, d.L. Heras et al. Solid State Commun., 74: 913(1990); https://doi.org/10.1016/0038-1098(90)90455-K

[3] E.A. Botchway, F.K. Ampong, I. Nkrumah, F.K. Boakye, R.K. Nkum, Open J. Appl. Sci. 9, 725(2019); https://doi.org/10.4236/ojapps.2019.99059

[4] M. Eghbalnia, D.G. Dixon, J. Solid State Electrochem. 17, 235(2013); https://doi.org/10.1007/s10008-012-1873-6

[5] P. Xiao, X.-L. Fan, H. Zhang, X. Fang, L.-M. Liu, J. Alloys Compd. 629, 43(2015); https://doi.org/10.1016/j.jallcom.2014.11.217

[6] I.J. Ferrer, C. Heras, C. Sanchez, Appl. Surf. Sci. 70-71, 588(1993); https://doi.org/10.1016/0169-4332(93)90585-Y

[7] I.J. Ferrer, C. Heras, C. Sanchez, J. Phys. Condens. Matter 7, 2115 (1995); https://doi.org/10.1088/0953-8984/7/10/018

[8] R. Chauhan, A. Kumar, R.P. Chaudhary, Spectrochim. Acta Part A 98, 256(2012); https://doi.org/10.1016/j.saa.2012.08.009

[9] G. Kaur, D. Pooja, M. Kumar, A. Thakur, R. Bala, A. Kumar, Phys. Chem. Chem.Phys.19,

32412(2017); https://doi.org/10.1039/C7CP06289C
[10] J.Y. Zhao, J.M. Zhang, J. Phys. Chem. C 121, 19334(2017); https://doi.org/10.1021/acs.jpcc.7b04568
[11] P. Diaz-Chao, I.J. Ferrer, C. Sanchez, Thin Solid Films 516, 7116(2008); https://doi.org/10.1016/j.tsf.2007.12.028
[12] G. Kaur, B. Singh, P. Singh, K. Singh, A. Thakur, M. Kumar, R. Bala, A. Kumar, Chem. Select 2, 2166(2017); https://doi.org/10.1002/slct.201700087
[13] W.L. Liu, X.H. Rui, H.T. Tan, C. Xu, Q.Y. Yan, H.H. Hng, RSC Adv. 4, 48770(2014); https://doi.org/10.1039/C4RA08527B
[14] M. Li, Q. Yao, G. Zhou, X. Qu, C. Mu, S. Fu, CrystEngComm 13, 5936(2011); https://doi.org/10.1039/c1ce05478c
[15] R. Ahuja, A. Sidhu, A. Bala, Eur. J. Plant Pathol. 155, 163(2019); https://doi.org/10.1007/s10658-019-01758-3
[16] S. Kawai, R. Yamazaki, S. Sobue, E. Okuno, M. Ichimura, Apl. Mater. 2, 032110(2014); https://doi.org/10.1063/1.4869035
[17] L. Charpentier, P. Masset, Mater. Sci. Forum 654-656, 2398 (2010); https://doi.org/10.4028/www.scientific.net/MSF.654-656.2398
[18] I.G. Orletskii, P.D. Mar'yanchuk, E.V. Maistruk, M.N. Solovan, V.V. Brus, Phys. Solid State 58, 37(2016); https://doi.org/10.1134/S1063783416010224
[19] S. Uchiyama, Y. Ishikawa, T. Doe, Y. Uraoka, IEEE International Meeting for Future of Electron Devices, Kansai (IMFEDK), pp. 28(2015); https://doi.org/10.1109/IMFEDK.2015.7158533
[20] R.J. Soukup, P. Prabukanthan, N.J. Ianno, A. Sarkar, C.A. Kamler, D.G. Sekora, J. Vac. Sci. Technol., A 29, 011001(2011); https://doi.org/10.1116/1.3517739
[21] M.L. Li, Q.Z. Yao, G.T. Zhou, X.F. Qu, C.F. Mu, S.Q. Fu, CrystEngComm 13, 5936(2011); https://doi.org/10.1039/c1ce05478c
[22] Z. Mutlu, B. Debnath, S. Su, C. Li, M. Ozkan, K.N. Bozhilov, R.K. Lake, C.S. Ozkan, J. Mater. Chem. C6, 4753(2018); https://doi.org/10.1039/C8TC00584B
[23] B.D. Cullity, S.R. Stock, Elements of X-ray Diffraction, third ed., Prentice-Hall, New Jersey (2001).
[24] M. Zebarjad, F. Jamali-Sheini, R. Yousefi, Ceram. Int. 47, 21969-21981(2021); https://doi.org/10.1016/j.ceramint.2021.04.215
[27] R. S. Ali, S. A. A. Mohammed, A. H. and Mohammed. IOP Conference Series: Materials Science and Engineering, , 928(7), 072154 (2020). https://**doi:** 10.1088/1757-899X/928/7/072154
[28] A. A. Khadayeir, E. S. Hassan, T. H. Mubarak, S.S. Chiad, N. F. Habubi, M.O. Dawood and I. A. Al-Baidhany. Journal of Physics: Conference Series, 1294 (2) 022009 (2019). https://doi: 10.1088/1742-6596/1294/2/022009
[29] V. Mote, Y. Purushotham, and B. Dole, J. Theor. and Appl. Phys., 6, 1-8(2012); https://doi.org/10.1186/2251-7235-6-6
[30] P. Chelvanathan, Y. Yusoff, F. Haque, M. Akhtaruzzaman, M. Alam, Z. Alothman, M. Rashid, K. Sopian, and N. Amin, Appl. Surf. Sci., 334, 138-144(2015); https://doi.org/10.1016/j.apsusc.2014.08.155
[31] C. De las Heras, J. de Vidales, I. Ferrer, and C. Sánchez, J. Mater. Res., 11, 211-220(1996); https://doi.org/10.1557/JMR.1996.0026
[32] R. Muhammad, A. M. Rana, M. Hafeez, E. Ahmed, A. S. Bhatti, M. F. Wasiq, M. Y. Nadeem. Acta Chim. Slov, 61, 80-86(2014).
[33] J. G. Yoon, H.K. Oh, and S.J. Lee, Phys. Rev. B, 60, 2839(1999).a. Adachi, A. Kudo1, T. Sakatal, Bull. Chem. Soc. Jpn. 68, 3283-3288(1995); https://doi.org/10.1103/PhysRevB.60.2839
[34] R. S. Ali, N. A. H. Al Aaraji, E. H. Hadi, N.F. Habubi and Chiad, S.S. Journal of Nanostructuresthis link is disabled, 10(4), 810–816 (2020).

https://doi: 10.22052/jns.2020.04.014
[35] R. S. Ali, M. K. Mohammed, A.A. Khadayeir, Z. M. Abood, N. F. Habubi and Chiad, S.S. Journal of Physics: Conference Series, 1664 (1), 012016 (2020).
https://doi:10.1088/1742-6596/1664/1/012016
[36] S.A. Darveau, In Proceedings of the 35th Photovoltaics specialists Conference, Institute of Electrical and Electronics Engineers (IEEE), pp. 002965-002969(2010).
[37] M. O. Dawood, S. S. Chiad, A. J. Ghazai3, N. F. Habubi and O. M. Abdulmunem. AIP Conference Proceedings 2213, 020102 (2020)
https://doi.org/10.1063/5.0000136
[38] E. S. Hassan, A. K. Elttayef, S. H. Mostafa, M. H. Salim and S. S. Chiad. Journal of Materials Science: Materials in Electronics 30 (17),15943-15951 (2019).
https://doi.org/10.1155/2014/684317
[39] E. S. Hassan, T. H. Mubarak, S. S. Chiad, N. F. Habubi, A. A. Khadayeir, M. O. Dawood and I. A. Al-Baidhany Journal of Physics: Conference Series, 1294 022008 (2019)
https://doi: 10.1088/1742-6596/1294/2/022008
[40] J. Tauc, Optical Properties of Amorphous Semiconductors, Plenum, New York, 1973;
https://doi.org/10.1007/978-1-4615-8705-7_4
[41] P. Prabukanthan and R. Dhanasekaran, Cryst. Growth Des. 7, 618-623 (2007);
https://doi.org/10.1021/cg060450o
[42] B.J. Lokhande, P.S. Patil, M.D. Uplane, Phys. B 302/303, 59-63(2001);
https://doi.org/10.1016/S0921-4526(01)00405-7
[43] D. R. Penn, Phys. Rev. 128, 2093 (1962); https://doi.org/10.1103/PhysRev.128.2093